Title

The influence of land cover on surface energy partitioning and evaporative fraction regimes in the U.S. Southern Great Plains

Journal

Journal of Geophysical Research: Atmospheres, 122(11)

ISSN

2169-897X

Authors

Bagley, Justin E
Kueppers, Lara M
Billesbach, Dave P
et al.

Publication Date

2017-06-16

DOI

10.1002/2017jd026740

Peer reviewed

The influence of land cover on surface energy partitioning and evaporative fraction regimes in the U.S. Southern Great Plains

Justin E. Bagley

Lara M. Kueppers

Dave P. Billesbach

Ian N. Williams

Sébastien C. Biraud
Margaret S. Torn
First published: 24 May 2017
https://doi.org/10.1002/2017JD026740
Cited by: 4
UC-eLinks

Abstract

Land-atmosphere interactions are important to climate prediction, but the underlying effects of surface forcing of the atmosphere are not well understood. In the U.S. Southern Great Plains, grassland/pasture and winter wheat are the dominant land covers but have distinct growing periods that may differently influence land-atmosphere coupling during spring and summer. Variables that influence surface flux partitioning can change seasonally, depending on the state of local vegetation. Here we use surface observations from multiple sites in the U.S. Department of Energy Atmospheric Radiation Measurement Southern Great Plains Climate Research Facility and statistical modeling at a paired grassland/agricultural site within this facility to quantify land cover influence on surface energy balance and variables controlling evaporative fraction (latent heat flux normalized by the sum of sensible and latent heat fluxes). We demonstrate that the radiative balance and evaporative fraction are closely related to green leaf area at both winter wheat and grassland/pasture sites and that the early summer harvest of winter wheat abruptly shifts the relationship between evaporative fraction and surface state variables. Prior to harvest, evaporative fraction of winter wheat is strongly influenced by leaf area and soil-atmosphere temperature differences. After harvest, variations in soil moisture have a stronger effect on evaporative fraction. This is in contrast with grassland/pasture sites, where variation in green leaf area has a large influence on evaporative fraction throughout spring and summer, and changes in soil-atmosphere temperature difference and soil moisture are of relatively minor importance.

1 Introduction

Land-atmosphere interactions are key components of the climate system. Current models, however, have limited ability to accurately represent surface energy partitioning and subsequent

coupling between land and atmosphere, particularly across different land covers [*Lawrence et al.*, 2007; *Zeng et al.*, 2010; *Pitman et al.*, 2011; *Dirmeyer et al.*, 2013]. Land cover, agricultural management, and urbanization can influence regional land-atmosphere interactions nonlinearly and generate regional biases in modeled climate metrics, including air temperature, cloud cover, and precipitation [*Xue et al.*, 1996; *Merrifield and Xie*, 2016; *Williams et al.*, 2016]. Surface energy partitioning and evaporative fraction (EF; defined as the latent heat flux normalized by latent plus sensible heat flux) exert a strong control on the state of the atmospheric boundary layer and translate variation in land surface properties to the atmosphere [*Findell et al.*, 2011; *Ford et al.*, 2014; *Williams and Torn*, 2015]. This can lead to perturbations of atmospheric quantities including precipitation, boundary layer height, lifted condensation level, and convective triggering [*Findell and Eltahir*, 2003; *Betts et al.*, 2007; *Berg et al.*, 2013; *Bagley et al.*, 2014a].

The Southern Great Plains (SGP) region of the United States is located in a transitional regime between wet and dry regions, and soil moisture varies over the year. Modeling studies have reported that precipitation and surface-energy partitioning in the SGP are more sensitive to variations in soil moisture than they are in other parts of the world, due in part to the SGP's transitional location [*Koster et al.*, 2004, 2006; *Seneviratne et al.*, 2006; *Dirmeyer*, 2011]. This has led to the conclusion that the SGP is a region of the world where land-atmosphere coupling may be particularly strong. However, observation-based studies of the relationship between soil moisture and surface energy and water fluxes do not corroborate this result; they suggest a weak influence of the land surface on the atmosphere in the SGP [*Ferguson and Wood*, 2012; *Phillips and Klein*, 2014]. At the same time, recent research found that land-atmosphere coupling in the SGP is controlled by factors beyond soil moisture and highlighted atmospheric factors such as wet versus dry conditions [*Santanello et al.*, 2013] and daily net radiation [*Ford et al.*, 2014]. Also, *Williams and Torn* [2015] and *Puma et al.* [2013] shifted the focus from soil moisture to the influence of vegetation, showing that surface energy partitioning is more strongly controlled by the state of vegetation, as represented by leaf area index (LAI), than by soil moisture. Their results suggest that the influence of the land surface on energy partitioning and potentially land-atmosphere coupling could be significantly stronger than earlier observational studies indicated and that the coupling may be driven by plant physiology and leaf phenology during the growing season. This is important because if surface forcing of the atmosphere and the terrestrial component of land-atmosphere coupling are strongly connected to vegetation, then land management and crop-growth timing could play important roles in the strength and origin of that forcing. However, the relative importance of drivers of variability in surface energy partitioning such as vegetation state, soil moisture, radiation, and others has not been quantified.

Additionally, the extent to which harvest timing and plant phenology influence the drivers of variability over the growing season and across major land cover types in the Southern Great Plains has not been assessed with observations.

In the SGP, the majority (85%) of land cover is either grassland (42%), which is often used as pasture and thus is referred to hereafter as grassland/pasture or cropland (43%); the primary crop is winter wheat (30% of total land cover) (U.S. Department of Agriculture (USDA) Cropscape Database, accessed October 2016 for the region shown in Figure 1). Winter wheat has a different growth cycle than other vegetation in the region; it is planted and emerges in fall and is typically harvested in May or June. As a result, winter wheat's maximum green leaf area occurs in April and May, and with the exception of weeds, the fields are largely bare during late summer. In contrast, grassland/pasture and other crops (e.g., maize and soybeans) in the region have small leaf area in April and May but grow through the summer. Crop growth cycles and harvest timing can influence surface fluxes of moisture, energy, and carbon [*Cooley et al.*, 2005; *Fischer et al.*, 2007; *Raz-Yaseef et al.*, 2015], but the influence of land cover on variability in surface forcing to the atmosphere has been largely neglected in studies of the SGP.

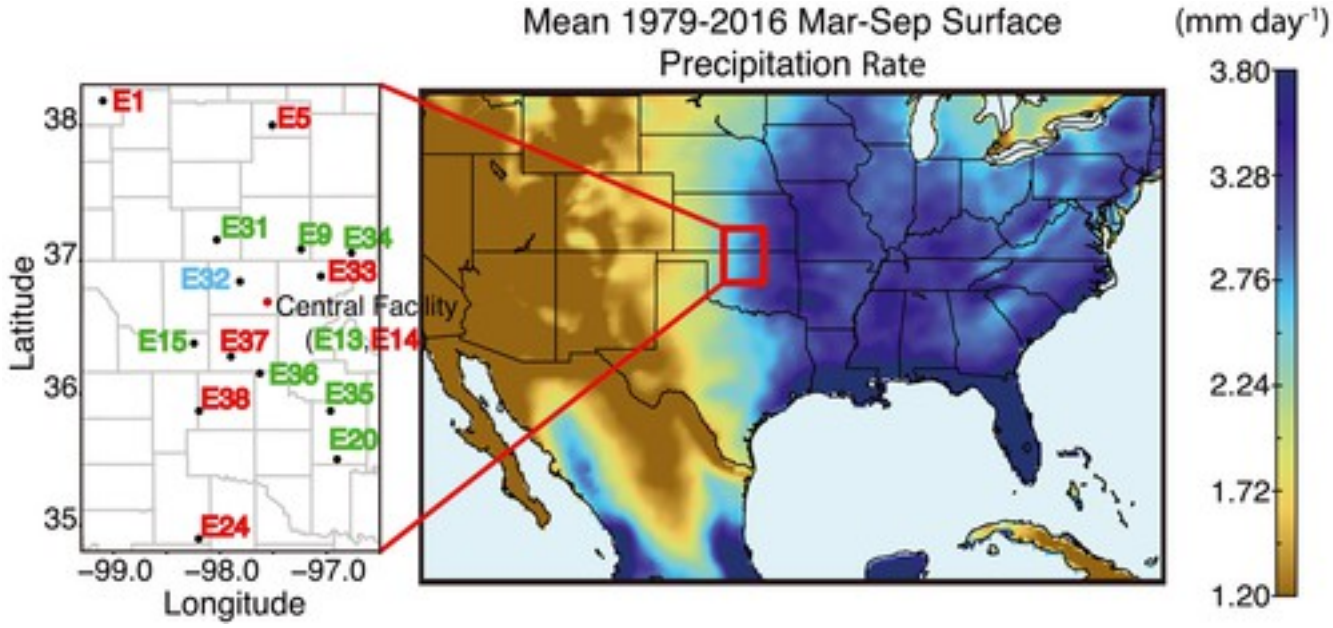

Figure 1

Open in figure viewerPowerPoint

Southern Great Plains domain and locations of surface flux sites used in this study. The shading shows the March–September 1979–2016 mean precipitation rate (data from North American Regional Reanalysis, NARR). The red labels indicate winter wheat sites, the green labels indicate grassland/pasture sites, and the blue label (E32) indicates a hayfield site.

Caption

Using largely statistically derived results, prior studies in the region [e.g., *Phillips and Klein*, 2014; *Ford et al.*, 2014; *Williams and Torn*, 2015] have shown that vegetation, soil moisture, and net radiation individually have important impacts on surface energy partitioning, evaporative fraction, and land-atmosphere coupling. However, a comprehensive study that investigates the relative importance of land surface, vegetation, and meteorology to evaporative fraction and the surface energy balance has not been previously conducted. Additionally, prior studies have not addressed the impacts that seasonally changing land cover has on the region. In particular, it is unknown how the early summer harvest of winter wheat, which directly alters the land cover and surface energy partitioning for a significant fraction of the Southern Great Plains, affects the response of evaporative fraction to changing meteorology and soil conditions. To address this knowledge gap, we compared the effects of preharvest and postharvest winter wheat and grassland/pastureland cover on spatial and temporal variations in surface albedo and evaporative fraction from March to September when regional variations in surface energy partitioning are expected to have the greatest influence on land-atmosphere coupling. Specifically, we statistically assessed multiple site-years of grassland/pasture and winter wheat data from the SGP using regression trees, random forests, and generalized additive models to assess the relationships between EF and surface metrics and to test how agricultural management of winter wheat influences these relationships.

2 Data and Methods

2.1 The Southern Great Plains Atmospheric Radiation Measurement Sites

We used March–September data from multiple surface energy flux measurement sites in Kansas and Oklahoma in this study (Figure 1). These sites are part of the U.S. Department of Energy Atmospheric Radiation Measurement (ARM) Southern Great Plains (SGP) Climate Research Facility. This facility consists of a central facility (CF) with a large suite of measurements and multiple extended facilities (ExFs) that are up to ~220 km from the CF with more limited measurements. These observational sites have been operating for various periods since 2002 (Table 1). The March–September period was chosen due to the potential importance of surface forcing to land-atmosphere coupling in the region during that time [*Koster et al.*, 2004].

Table 1. Southern Great Plains Surface Flux Measurement Locations and Land Cover Type Used in This Study

Site Location	Abbreviation	Flux Data Availability	Primary Crop/Vegetation
Larned, KS	E1	2003–2009	Winter wheat
Leroy, KS	E3	2003–2009	Winter wheat
Halstead, KS	E5	2003–2008	Winter wheat
Ashton, KS	E9	2003–2015	Grassland/pasture
Centr. Fac., OK	E13	2002–2015	Grassland/pasture
Centr. Fac., OK	E14	2002–2015	Winter wheat
Ringwood, OK	E15	2003–2015	Grassland/pasture
Meeker, OK	E20	2003–2011	Grassland/pasture
Cyril, OK	E24	2003–2009	Winter wheat[a]
Medford, OK	E32	2011–2015	Hayfield[b]
Newkirk, OK	E33	2011–2015	Winter wheat-soy (double crop)
Anthony, KS	E31	2011–2015	Grassland/pasture[c]

Site Location	Abbreviation	Flux Data Availability	Primary Crop/Vegetation
Maple City, KS	E34	2011–2015	Grassland/pasture
Tyron, OK	E35	2011–2015	Grassland/pasture
Marshall, OK	E36	2011–2015	Grassland/pasture
Waukomis, OK	E37	2011–2015	Winter wheat
Omega, OK	E38	2011–2015	Winter wheat

- a At E24, only 2 years (2003–2004) of winter wheat data were available. The vegetation type for other years was unclear from field reports.
- b This site was only used for comparison between EBBR and ECOR systems.
- c The ECOR system used at E31 differed from other grassland/pasture sites that used EBBR systems. See section 2.2 for details on ECOR and EBBR systems.

The network of surface flux sites is located on an east-west precipitation gradient, with the western sites being relatively dry (~1.8 mm d^{-1} mean annual precipitation rate) compared to those in the east (~2.5 mm d^{-1} mean annual precipitation rate) [*Raz-Yaseef et al.*, 2015]. The land cover in the region is primarily winter wheat and grassland/pasture (Table 2), which is a mix of C_3 and C_4 grasses [*Fischer et al.*, 2007]. The ARM flux sites that we used for this analysis were over winter wheat or grassland/pasture (Table 1). However, the winter wheat sites were intermittently rotated to other crops, and some crop sites were occasionally fallow. Additionally, double-cropping (where winter wheat is harvested and, another crop, typically soy, is planted immediately afterward and harvested in fall) occurs intermittently at several of the sites. Biweekly field reports were available for all sites. These reports detailed land cover type, approximate vegetation height, and vegetation conditions. These reports were used to determine crop type during each growing season (including whether a second crop was sown after wheat

was harvested) and to estimate emergence and harvest dates of each field. We excluded years in which winter wheat was not grown. Finally, we defined winter wheat preharvest and postharvest periods based on the date of winter wheat harvest. This date was determined using observed harvest dates from biweekly field reports, and the periods were defined as the 60 days preceding or following harvest, respectively. The week before and after the estimated harvest date was discarded due to uncertainty of the exact harvest date from biweekly field reports. In order to compare winter wheat and grassland/pasture sites during concurrent periods, we divided the grassland/pasture data based on winter wheat's preharvest and postharvest periods. At the CF grassland/pasture field, we defined the prewinter wheat harvest and postwinter wheat harvest periods to be identical to that observed at the adjacent winter wheat site. For the other grassland/pasture sites, which did not have adjacent winter wheat fields, we defined pre and post winter wheat harvest periods based on the mean harvest date across all SGP winter wheat sites for a given year.

Table 2. Primary Land Cover Types in the Southern Great Plains Study Domain During 2015 (USDA). The “Other” Category Is Primarily a Mix of Minor Crops

Land Cover	% of Total Area
Pasture/grassland	42
Winter wheat	30
Deciduous forest	6
Developed	4
Corn	3
Sorghum	3

Land Cover	% of Total Area
Soybeans	3
Other	9

2.2 Flux, Soil, and Meteorological Measurements in the SGP

At the winter wheat ExFs, fluxes of water, energy, and carbon were observed using eddy correlation (covariance thereafter) flux measurement systems (ECOR) [*Cook*, 2016a]. ECOR systems were used since they can measure fluxes from the edge of fields and would reduce interference with agricultural activities. The measurements provided estimates of half-hourly net fluxes of momentum, sensible heat, latent heat, and carbon dioxide. The eddy covariance instruments are typically located on the northern edge of fields, so that the fetch sampled the crop during prevailing southerly winds. Fluxes and other quantities measured during periods with nonsoutherly wind directions were filtered out for this study, as were days with significant precipitation, which can compromise flux estimates (~17% of total data at CF). The uncertainty of ECOR flux measurements for landscapes similar to the Southern Great Plains is typically ~10% [*Finkelstein and Sims*, 2001; *Massman and Lee*, 2002; *Billesbach*, 2011]. Combined with solar radiation and soil microclimate measurements, these systems have 75–90% closure for surface energy balance [*Twine et al.*, 2000]. The residuals are often due to a combination of unmeasured dissipative terms such as canopy energy storage, instrument limitations, and variations in atmospheric conditions [*Twine et al.*, 2000; *Massman and Lee*, 2002]. It is often believed that this lack of energy closure can lead to underestimates of sensible and latent heat fluxes using the eddy covariance measurement technique. It is, however, just as plausible that dissipative terms that are not measured can cause overestimates of the available energy (net radiation, soil heat flux, and other terms). However, we assumed that the impact of energy closure and measurement uncertainty on surface fluxes and EF is small relative to the variability in fluxes associated with environmental changes.

At the grassland/pasture CF and ExFs, surface fluxes were measured using energy balance Bowen ratio (EBBR) systems [*Cook*, 2016b]. These systems use observations of net radiation, soil energy storage, and gradients of temperature and vapor pressure to estimate sensible and

latent heat fluxes with instrumental uncertainty of ~10% [*Fritschen and Simpson*, 1989]. This method forces perfect closure of the surface energy balance. One drawback of EBBR systems is their inability to independently measure sensible heat flux (H), latent heat flux (LE), and available energy. Unlike eddy covariance systems where H and LE can be compared to independently measured available energy, all energy components from EBBR systems derive from the same set of measurements. Additionally, measurement footprint remains a concern. Similar to the ECOR measurements, observations from periods with wind directions not representative of the local land cover (grassland/pasture) were filtered from the analysis, as were days with precipitation.

The two types of instrumentation (EBBR and ECOR) are deployed at the same location at one hayfield site near Medford, OK. Figure 2 shows comparisons of 30 min sensible heat flux, latent heat flux, and midday (10:00–14:00 CST; UTC 6 h) EF values between the two instrument systems for January–August 2016, when both were operating. The slopes for latent and sensible heat flux are both within 3% of the 1:1 line, and the R^2 values indicate good linear relationships. This is consistent with other comparisons made in similar short-statured ecosystems [*Billesbach and Arkebauer*, 2012]. While there is scatter around the fit line, longer term (daily, weekly, monthly, etc.) averages are expected to converge toward the line. EF has similar scatter around the line of best fit, and the best fit line's slope deviates more from the 1:1 line, but the R^2 remains above 0.7. In short, this method's comparison gives confidence in our use of energy flux measurements from both ECOR and EBBR measurement systems in a common analysis and that instrument effects on measurements of EF are small.

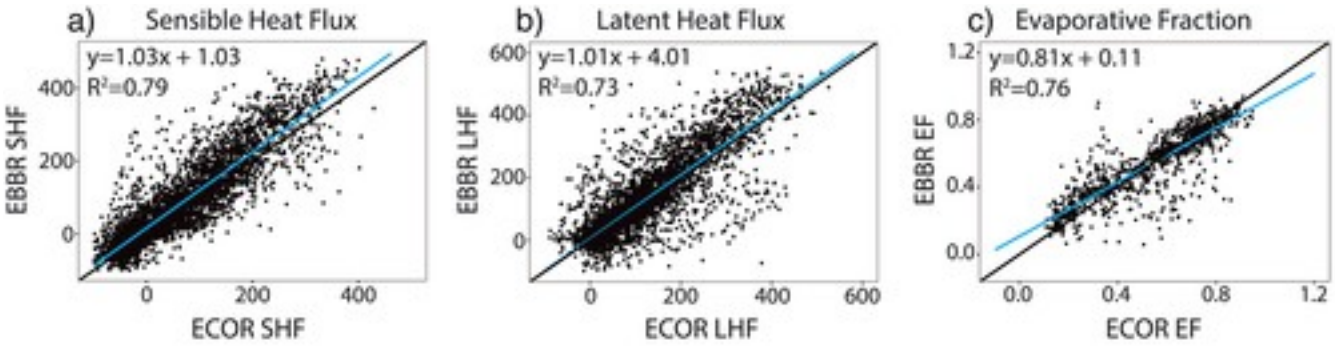

Figure 2
Open in figure viewerPowerPoint
Comparison of midday (10:00–14:00 CST; UTC 6 h) (a) sensible heat flux (SHF), (b) latent heat flux (LHF), and (c) evaporative fraction (EF) measured by co-located ECOR and EBBR instruments at hayfield site in Medford, OK (E32 in Figure 1) during 2016.
Caption

Meteorological instruments are co-located with the majority of ECOR and EBBR instruments used in this study. These measured 2 m temperature (Vaisala HMP45C), precipitation rate (NovaLynx TBRG), 10 m wind speed (RM Young 05103) and wind direction (RM Young 05103), and 2 m relative humidity (Vaisala HMP45C) every minute. The data were averaged over 30 min periods for analysis. Additionally, vertical profiles of volumetric soil moisture and temperature were measured using Campbell Scientific 229 L Soil-Water Potential Sensors at a couple of locations and at multiple depths ranging from 5 to 60 cm at most sites, and deeper measurements were available at some locations (Soil and Water Temperature System, SWATS) [*Cook*, 2016c]. Soil measurements were averaged to hourly values at each depth and filtered for data quality. For this study, only volumetric soil moisture measurements for the top 30 cm were used. These depths were available for all sites. For the purposes of the remainder of this study, "soil moisture," or θ_v, refers to volumetric soil moisture for the top 30 cm.

2.3 The ARM-SGP Central Facility

At the ARM-SGP CF, concurrent surface flux measurements have been taken since 2003 at adjacent agricultural and grassland/pasture sites (sites are ~350 m apart) that experienced identical weather (Figure 1 and E13 and E14 in Table 1). The agricultural field was primarily winter wheat, but different crops were planted in 2005 (maize), 2008 (maize), 2010–2011 (canola; a winter crop with phenology similar to winter wheat), and 2015–2016 (alfalfa). Additionally, soy was planted following winter wheat harvest during 2006, and cowpeas followed winter wheat harvest in 2012 and 2013.

Measurements taken at the CF include those described in section 2.2. However, additional measurements have been made at this location for both fields. Within the agricultural (primarily winter wheat) field are instruments that provide measurements of surface fluxes at 30 min resolution using eddy covariance measurements mounted at 4 m (CO2FLX; Gill Windmaster Pro) [*Fischer*, 2005]. Also, near the CO2FLX system (<30 m away), the agricultural field soil moisture and soil temperature were measured at 5, 15, and 25 cm depth using Decagon ECH2O soil moisture sensors and Type-E thermocouples. The CO2FLX soil moisture measurements appeared to retain sensitivity to soil moisture variations outside of those measured by the SWATS instrument at the neighboring grassland/pasture field. However, during the periods used in our analysis, <5% of data was from outside the range of SWATS sensitivity and restricting our analysis to periods when both SWATS and CO2FLX that were sensitive had a negligible influence on our results. Additionally, soil moisture readings at the grassland/pasture site (E13) had a physically unrealistic step change during 2009. As a result, all analyses using CF soil moisture were limited to 2003–2008. Finally, spectral reflectance at near-infrared (870 nm) and

red (673 nm) wavelengths were available at 25 m from the 60 m tower as well as from the top of a 10 m tower located in the grassland/pasture site from 2003 to 2011. Using the data in conjunction with intermittent direct measurements of leaf area index (LAI) using a LI-COR LAI-2000 Plant Canopy Analyzer [*Fischer et al.*, 2007], daily estimates of leaf area index (LAI) for the crop and grassland/pasture sites were derived following *Baret and Guyot* [1991], as described in *Williams and Torn* [2015]. Unlike analyses requiring soil moisture, analyses of LAI and albedo (i.e., Figures 4 and 5) were unaffected by the inconsistent soil moisture measurements in 2009, so we used all available data (2003–2011) for these analyses.

2.4 Statistical Analysis

We applied regression trees, random forests, and generalized additive models (GAMs) to assess the relationships between EF and surface metrics and to test how agricultural management of winter wheat influences these relationships. This portion of the analysis was limited to the central facility due to the lack of measurements suitable for estimating LAI at other sites in the ARM-SGP. The surface metrics we used as explanatory variables for EF included leaf area index (LAI; $m^2\ m^{-2}$), volumetric soil moisture (θ_v; $m^3\ m^{-3}$), land-atmosphere temperature difference (T_{diff}; °C), 2 m relative humidity (RH; %), wind speed (U; $m\ s^{-1}$), net radiation (R_n; $W\ m^{-2}$), surface energy storage (G; $W\ m^{-2}$), and an error term (ε). i.e.:

$$EF = f(LAI, \theta_v, T_{diff}, RH, U, R_n, G) + \varepsilon \quad (1)$$

The soil moisture and temperature (T_{soil}) were taken from the top level of soil measurements (~0–10 cm). The sign convention of T_{diff} was defined by

$$T_{diff} = T_{soil} - T_{air} \quad (2)$$

where T_{air} is the 2 m air temperature. These explanatory variables had low collinearity, with estimates of variance inflation factors for this set of variables all having values less than 1.5. The overall goals of this approach were to (1) identify regimes for which the primary determinants of EF change (e.g., high θ_v versus low θ_v), (2) assess the relative importance of explanatory variables under varied regimes, and (3) quantify statistical relationships between important explanatory variables and ET for varied regimes.

Regression trees explain variation in a response variable by repeatedly splitting or “branching” the data into increasingly homogenous groups that minimize the sum of squares errors, with each split based on a single explanatory variable and each grouping characterized by a mean value or distribution of the response variable (EF for this study) [*Death and Fabricius*, 2000]. The resulting regression tree can be represented graphically with the root node at the top representing the entirety of data and subsequent branches and nodes below. This method reveals natural splits

in the relationships between the response and explanatory variables. To avoid overfitting, the regression tree is limited to a set number of splits or pruned to retain explanatory power on training and testing data. We used the “rpart” R package for regression tree analysis [*Therneau et al.*, 2010].

Random forests extend regression trees by iteratively randomizing the explanatory variables that each tree is allowed to use. For each tree in the ensemble (500 ensemble members for this study), a bootstrapped subset of data (63% of the full data set) is drawn from training data (with the excluded data being “out-of-bag”). Then, at each node of the tree, a random subset of explanatory variables (three in our study) is chosen from the total available variables and the best possible split of data is determined. This process continues until each tree is fully grown [*Zumel and Mount*, 2014]. By taking advantage of the large number of bootstrapped ensemble members and out-of-bag data used in this method, the importance of individual explanatory variables can be evaluated by considering the decrease in model accuracy with that variable's exclusion [*Zumel and Mount*, 2014]. We used the “randomforest” R package for random forest calculations [*Liaw et al.*, 2009].

We used generalized additive models (GAMs) with the R package “mgcv” [*Wood*, 2012] to investigate nonlinear relationships between the explanatory surface variables and EF. GAMs are similar to linear models in that they simultaneously fit functions of explanatory variables to minimize model error. However, GAMs allow nonlinear functions, in our case splines, to be fit. The resulting functions can be graphically presented to assess relationships between the explanatory land surface variables and EF. For the full March–September study period the fitted GAM models were able to explain much of the variance in EF for grassland/pasture (Figure 3b) and winter wheat (Figure 3a) with R^2 values of 0.76 and 0.57, respectively (Figure 3). The apparent clustering in Figure 3a (winter wheat) is likely due to the impact of harvest and the reduction of the influence of LAI after harvest.

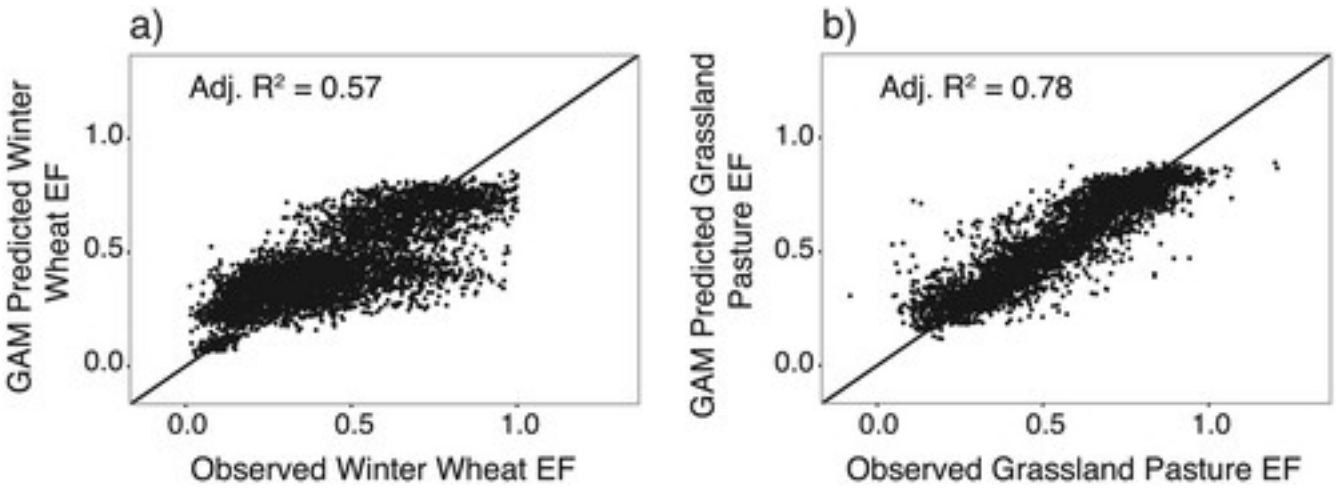

Figure 3

Open in figure viewerPowerPoint

Comparison of GAM predicted (a) winter wheat and (b) grassland/pasture evaporative fraction (EF) with measurements at the central facility (CF).

Caption

3 Results

3.1 Impacts of Land Cover on Leaf Area, Net Radiation, and Surface Energy Partitioning

The timing of leaf area for winter wheat differed markedly from that of summer-active grassland/pasture (Figure 4). With a mean planting date of early October, winter wheat at the CF emerged in late October and commonly reached a seasonal maximum green leaf area of ~1–1.5 m^2 m^{-2} in December that was maintained through February, with some decreases that may be attributable to extreme cold events. As the likelihood of cold events decreased and radiation increased in late February, winter wheat green leaf area increased, reaching a maximum of ~3.0–4.0 m^2 m^{-2} in late April as the crop matured. During this period, plants allocated resources to grain, which led to gradual leaf browning, senescence, and a sharp decrease in green LAI. Finally, harvest generally occurred in late May to early June. According to field reports, the LAI remained close to zero until significant weeds emerged. Weeds commonly contributed to a second, smaller maximum in leaf area in late summer, which was later eliminated as the soil was prepared for planting. This is evident in the small rise in winter wheat LAI during mid-July in Figure 4. However, it should be noted that the increase in LAI is not consistent across years, as indicated by the increased spread in LAI during this time.

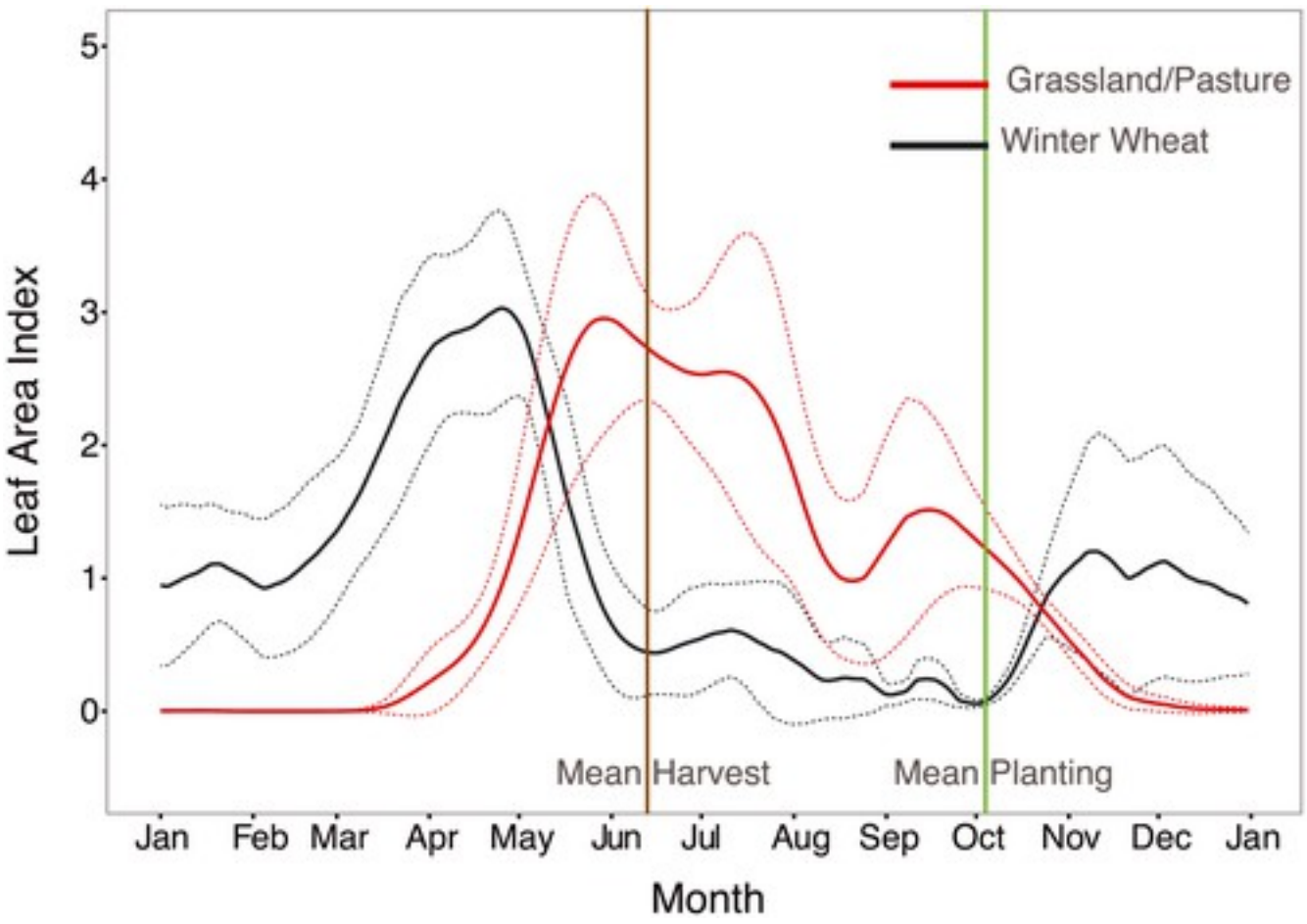

Figure 4

Open in figure viewerPowerPoint

Mean LAI for grassland/pasture (red lines) and winter wheat (black lines) from 2003 to 2011 at the central facility (CF). The solid lines are mean values, and the dashed lines show one standard deviation. The vertical lines indicate mean harvest (brown) and planting (green) dates.

Caption

Grassland/pasture leaf phenology at the central facility was dictated by the genetics of the local C_3 and C_4 grasses, their responses to meteorological conditions, and agricultural management. The grassland/pasture emerged from dormancy in April, and green leaf area increased consistently to a summer maximum ~3–3.5 m^2 m^{-2} that was irregularly reduced by mowing or cattle grazing (Figure 4). Fall senescence reduced the grassland/pasture green leaf area from August through November. The differences in phenology and management between winter wheat and grassland/pasture led to large seasonal differences in LAI. These differences were particularly large (up to ~3 m^2 m^{-2}) in spring when winter wheat reached its maximum LAI and grassland/pasture was emerging from winter dormancy. The opposite occurred during summer, after winter wheat harvest, as the grassland/pasture reached its maximum LAI and the winter wheat field had minimal vegetation.

Differences in the annual growth cycles of winter wheat and grassland/pasture had impacts on the surface energy balance. Figures 5a and 5b show the observed preharvest and postharvest associations between daytime (900–1500 CST) albedo and LAI at the CF grassland/pasture and winter wheat sites. Prior to winter wheat harvest, the LAI of the winter wheat was typically greater than that of the grassland/pasture. Additionally, the albedo of the winter wheat site was greater, such that winter wheat absorbed up to ~13% less shortwave radiation than the neighboring grassland/pasture. Conversely, after the winter wheat harvest, the land cover of the winter wheat field consisted of bare soil and intermittent weeds. This led the winter wheat field to have a reduced albedo, while the grassland/pasture site was reaching its maximum LAI and had an albedo up to 0.1 greater than that of the winter wheat site. Periods of greatest LAI difference also had the largest difference in albedo.

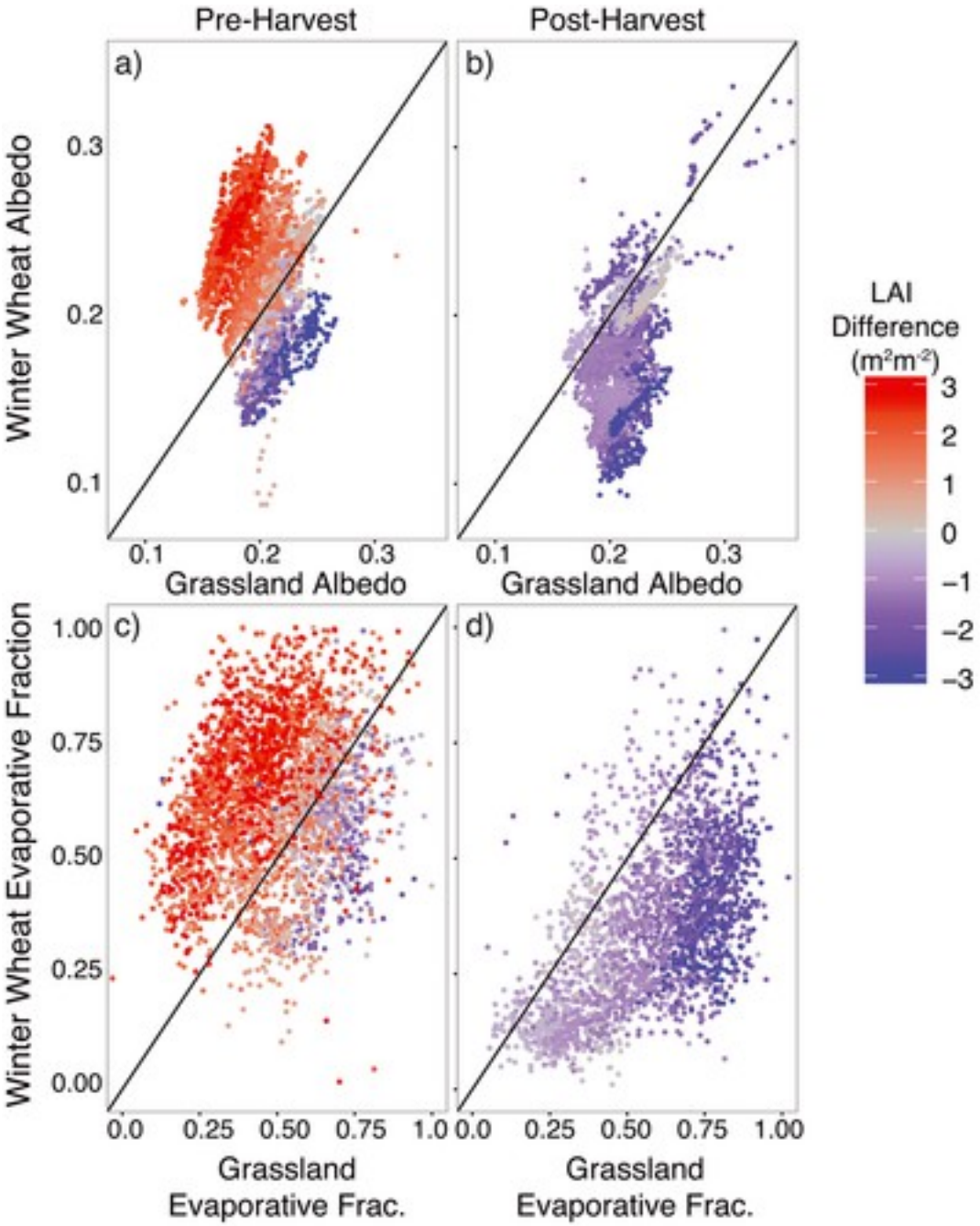

Figure 5

Open in figure viewerPowerPoint

Relationship between winter wheat and grassland for (a and b) preharvest and postharvest albedo and (c and d) evaporative fraction at the central facility. The shading illustrates the difference in LAI (winter wheat minus grassland/pasture).

Caption

The seasonal differences in leaf area between winter wheat and grassland/pasture led to seasonal differences in latent and sensible heat fluxes and thus EF. As shown in Figures 5c and 5d, during the winter wheat preharvest periods for 2003–2011, the evaporative fraction of the winter wheat

field was ~0.4–0.6 greater than the adjacent grassland/pasture field, and the opposite occurred postharvest when winter wheat LAI was minimal. The greatest differences in latent heat flux occurred during the spring when the winter wheat site had significantly greater moisture fluxes than the grassland/pasture site, while the largest differences in sensible heat flux followed the early summer harvest of winter wheat with the grassland/pasture site having low sensible heat fluxes during this period (~25 Wm^{-2}) relative to the winter wheat site (~80–100 Wm^{-2}).

3.2 Drivers of Evaporative Fraction Variation

Variation in winter wheat EF between March and September was explained by variations in LAI, soil moisture (θ_v), and soil-air temperature differences (T_{diff}). Regression tree analysis for 2003–2008 data from the CF winter wheat field (Figure 6) indicated that when the LAI was below 1.5 $m^2\ m^{-2}$, θ_v was an important determinant of EF, but as the LAI increased above 1.5 $m^2\ m^{-2}$, T_{diff} became an important variable. The periods when the winter wheat field had an LAI < 1.5 $m^2\ m^{-2}$ generally represented the postharvest period from ~June to September, while periods when LAI was >1.5 $m^2\ m^{-2}$ largely corresponded to preharvest periods. This implies that when winter wheat was harvested, θ_v was an important factor in determining EF, but for preharvest, when the LAI was above 1.5 $m^2\ m^{-2}$, the direct effect of θ_v was less important.

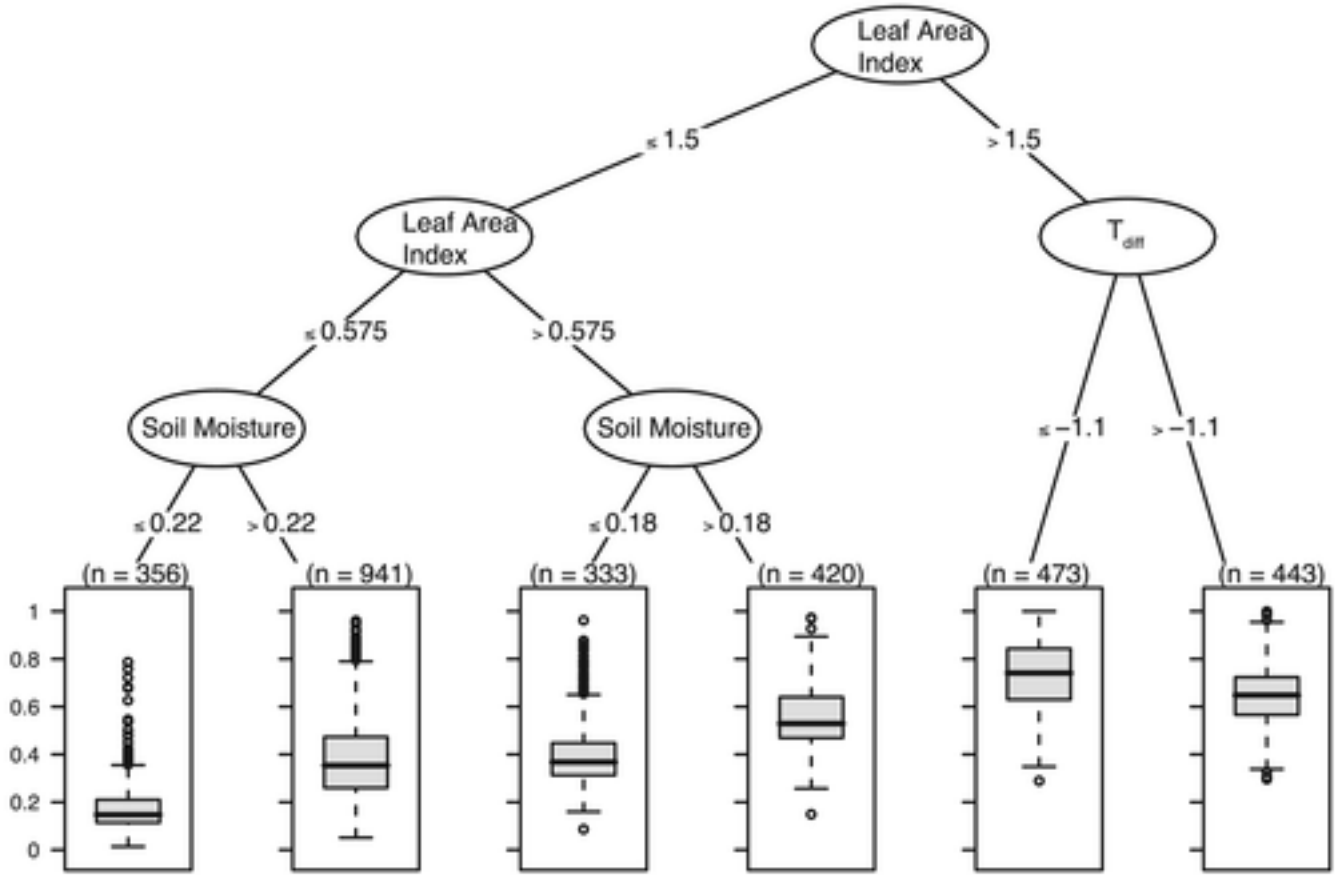

Figure 6

Open in figure viewerPowerPoint

Central facility regression tree for winter wheat evaporative fraction using data from 2003–2008 and variables given in equation 1. The bottom row box and whisker diagrams indicate number of data points in each node and distribution of evaporative fraction values in each node.

Caption

For the CF winter wheat and grassland/pasture sites, the derived random forest models were able to explain ~90% of the variance (Table 3). When the data were subdivided into periods of low and high LAI, the percentage of variance explained decreased for the winter wheat site but remained above 75%. The above result that LAI, θ_v, and T_{diff} had the greatest influence on EF variation was reinforced using estimates of variable importance derived from random forest analysis, which similarly showed that θ_v, T_{diff}, and LAI were the most important explanatory variables of EF (Table 3). Additionally, GAM fitted functions for LAI, θ_v, and T_{diff} illustrate the functional dependence of EF on these variables (Figures 7a–7c). Increasing LAI led to greater EF in winter wheat, although this appears to saturate around 2.0 m^2 m^{-2} (Figure 7a).

At $\theta_v < 0.25$ m^3 m^{-3}, EF increased nearly linearly with soil moisture (Figure 7b). However, above 0.25 m^3 m^{-3}, the impact of soil moisture on EF was reduced. For −5°C < T_{diff} < 0°C, increases in T_{diff} corresponded to small decreases in EF due to increasing sensible heat flux but were otherwise small.

Table 3. Random Forest Variable Importance Calculated as the Percentage Increase in Model Mean Square Error of EF With Each Variable Removed[a]

	Winter Wheat Site (E14)			Grassland Pasture Site (E13)		
Variable	**All Data**	**Preharvest**	**Postharvest**	**All Data**	**Preharvest**	**Postharvest**
LAI	**178.9**	**124.5**	**110.6**	**145.0**	**83.3**	**95.0**
θ	**124.6**	**42.3**	**105.6**	**52.2**	**31.5**	**42.1**
T_{diff}	**95.4**	**97.0**	**62.9**	**59.5**	**35.1**	**45.9**
U	51.7	33.1	43.0	32.7	23.9	30.6
G	54.6	37.5	43.4	38.2	21.8	32.6
RH	54.2	**42.3**	41.1	45.7	28.9	39.5
R_n	40.4	40.8	25.5	33.9	22.5	30.1
% var.	89.8	88.7	88.1	91.2	91.9	89.9

- a Each column represents a separate model fit of EF as a function of the listed variables. The bold values indicate the three most important variables for each case. Also shown is the overall model variance explained by the regression tree for each case.

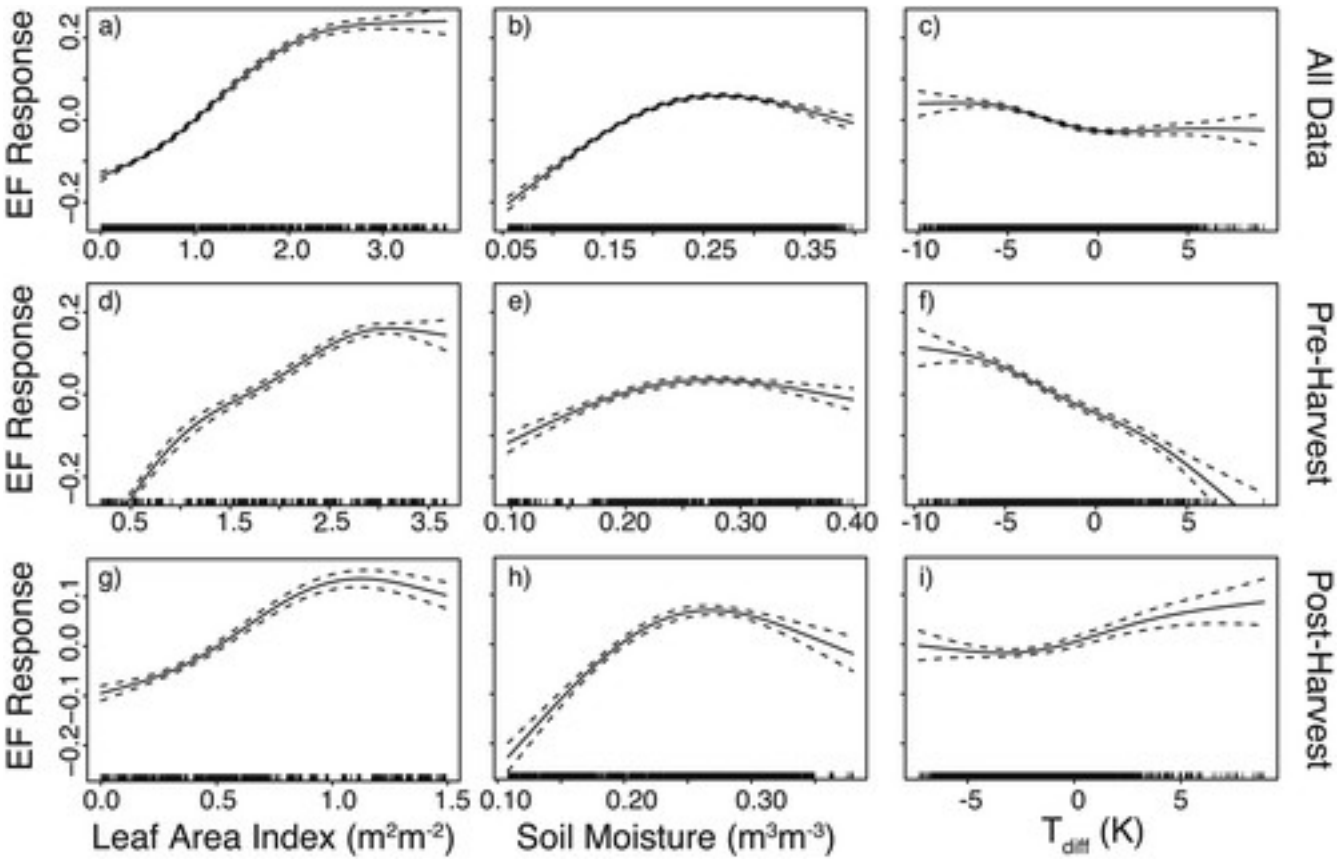

Figure 7

Open in figure viewerPowerPoint

Evaporative fraction response curves from general additive models for winter wheat LAI, volumetric soil moisture, and T_{diff} at the central facility during (a–c) full March–September period, (d–f) preharvest, and (g–i) postharvest. The negative (positive) values of EF response for LAI, volumetric soil moisture, or T_{diff} indicate that the respective terms of the GAM model reduced (increased) EF for those values of the predictors. The *x* axis tick marks indicate observational locations used in the GAM model.

Caption

Given the strong effects of harvest on leaf area index and EF, we split the winter wheat data based on observed harvest date as described in section 2.1 to quantify the relative importance of land surface variables during winter wheat preharvest and postharvest periods. After separating the data, LAI remained the most explanatory variable of winter wheat EF variation (Table 3). However, postharvest, the importance of θ_v was greatly increased relative to other variables. On the other hand, for preharvest, T_{diff}'s importance was strongly enhanced. The GAM-fitted functional relationships of these variables with EF are shown in Figures 7d–7i. Similar to the full March–September results, for the preharvest and postharvest periods, increased LAI corresponded to increased EF. Additionally, for preharvest, the dependence of EF on θ_v was reduced, while for postharvest, it increased, as seen in the differences in slopes of the curves when soil moisture is <0.25 $m^3\ m^{-3}$ (Figures 7e and 7h). Finally, for preharvest, there was a strong

negative relationship between EF and T_{diff} (Figure 7f), and for postharvest, there was no clear pattern for T_{diff}, and random forest analysis indicated that T_{diff} had limited importance (Figure 7i). This may be due to the increased importance of soil moisture in the absence of vegetation.

The above analysis of winter wheat indicates that land cover and land management (harvest) appear to play an important role in determining the controls on surface energy partitioning in the Southern Great Plains. However, these changes could be due to changes in seasonal meteorology. To control for this, we assessed the importance of variables at the adjacent grassland/pasture site during identical periods. At the grassland/pasture site from March to September, the surface variables explaining variation in EF were the same as those in the winter wheat site (Table 3), with LAI most important, followed by soil moisture and air-soil temperature difference. Similarly, as shown in Figures 8a–8c, the functional responses of EF to these variables were similar to those for winter wheat. There was a strong dependence of EF on LAI up to ~3 m^2 m^{-2}, after which the dependence appeared to saturate. EF increased almost linearly with soil θ when θ_v was less than ~0.28 m^3 m^{-3}, and the negative relationship between EF and T_{diff} remained. However, in contrast to the winter wheat site, at the grassland/pasture site during the pre and post winter wheat harvest periods, θ_v and T_{diff} were only slightly more important for explaining variations in EF, and their relative importance did not significantly change before and after harvest (Table 3). This indicated that the preharvest and postharvest differences observed at the winter wheat site were due to changes in land cover and not seasonal meteorology. Finally, Figures 8d–8i present the GAM functional fits of LAI, θ_v, and T_{diff} for the grassland/pasture site during the pre and post winter wheat harvest periods. Overall, they were consistent with the functions derived for the full March–September period. The exception was that prewinter wheat harvest soil moisture appears to have minimal influence on EF at the grassland/pasture site (Figure 8e).

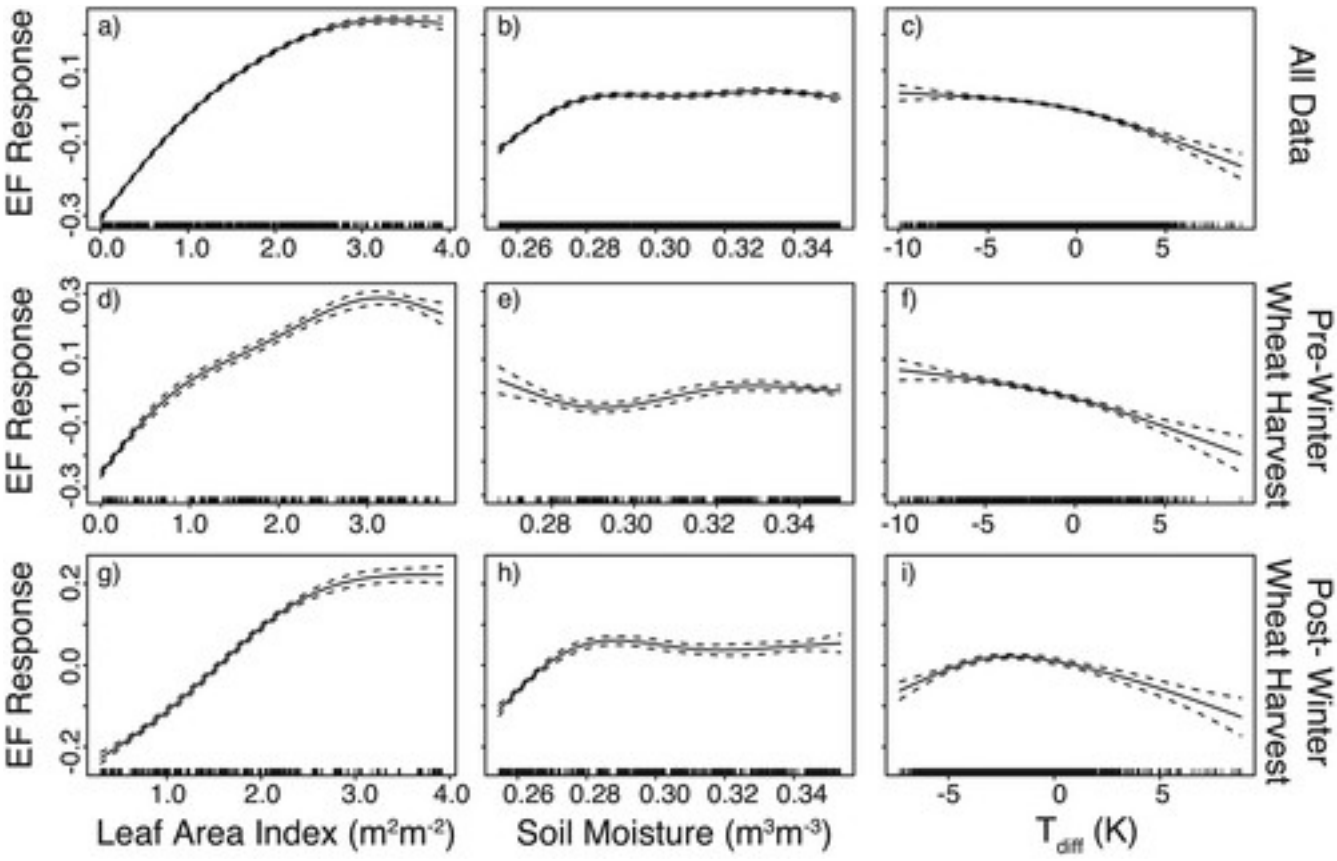

Figure 8

Open in figure viewerPowerPoint

Evaporative fraction response curves from general additive models for grassland/pasture LAI, volumetric soil moisture, and T_{diff} at the central facility during (a–c) full March–September period, (d–f) prewinter wheat harvest, and (g–i) postharvest. The negative (positive) values of EF response for LAI, volumetric soil moisture, or T_{diff} indicate that the respective terms of the GAM model reduced (increased) EF for those values of the predictors. The *x* axis tick marks indicate observational locations used in the GAM model.

Caption

3.3 Regional Impact of Winter Wheat Harvest on Evaporative Fraction and Albedo

We analyzed EF and albedo data across multiple grassland/pasture and winter wheat sites to gain insight into whether the shift in EF and albedo at harvest found at the CF was consistent across other sites and to see if the dependency of pre/postharvest EF on surface variables shown at the CF extended across the region. The pre and postwinter wheat harvest probability distributions of EF and albedo across all winter wheat and grassland/pasture sites within the ARM SGP facility (Table 1) from 2002 to 2015 show that the preharvest and postharvest distributions of EF were distinct between winter wheat and grassland/pasture sites (Figure 9), similar to the results from the CF. The EF in winter wheat fields was larger in the preharvest period (mean EF ~ 0.55) than

in the postharvest period (mean EF ~ 0.34), while the opposite shift occurred at the grassland/pasture sites. For albedo, the differences in preharvest and postharvest distributions of EF were subtler. Similar to the CF, across all winter wheat sites, the albedo was likely to slightly decrease following harvest, and at grassland/pasture sites, the difference in albedo was negligible between pre and postwinter wheat harvest periods.

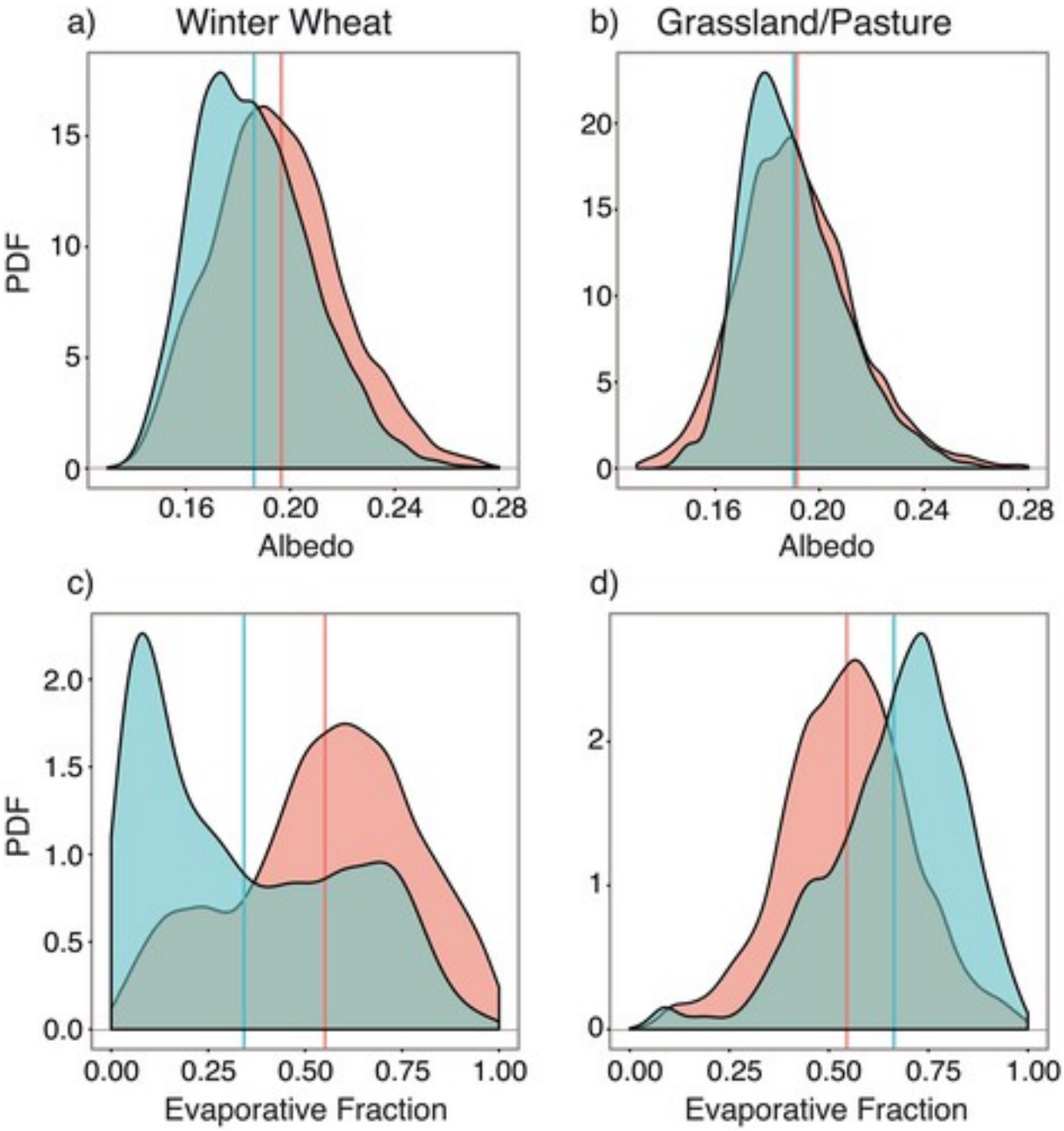

Figure 9
[Open in figure viewerPowerPoint]

Probability distribution of (a and b) prewinter wheat harvest (red) and postwinter wheat harvest (blue) albedo and (c and d) evaporative fraction for winter wheat (seven sites, Figures 9a and 9c) and grassland/pasture (seven sites, Figures 9b and 9d) sites across the Southern Great Plains from 2003 to 2015. The red and blue lines indicate mean values of albedo and evaporative fraction across all sites in the ARM-SGP during pre and post winter wheat harvest periods.
Caption

4 Discussion

The distinct phenology and management of winter wheat relative to other land cover types in the SGP produce a unique seasonal pattern of LAI, absorbed solar radiation, and EF during much of the March–September period. The May–June senescence and harvest of winter wheat represented essentially a step change in summer LAI that did not occur in grassland/pasture, the other dominant vegetation type in the region. We found that land surface forcing of the atmosphere is sensitive to these differences in crop type and management. Using multiple years of observations, we have shown that the phenology and harvest timing of winter wheat influence EF and radiative balance across the region. Prior to harvest, the EF of winter wheat could be up to ~40–60% larger than that of neighboring grassland/pasture, while after harvest, EF was larger for grassland/pasture. This confirms earlier work by *Fischer et al.* [2007] who showed for a single year that the differences between these land cover types in latent and sensible heat fluxes both reached ~50–75 Wm^{-2}. Similarly, differences in albedo demonstrated that the total radiative energy absorbed by winter wheat was low relative to grassland/pasture prior to harvest and high relative to the grassland/pasture after harvest. Although the differences in albedo were small, they are likely to be important for the overall energy balance for different land cover types.

At the CF winter wheat site, LAI was the most influential determinant of EF from March to September. However, when we split the data into preharvest and postharvest periods, the importance of other variables emerged. Since leaf area was small postharvest, the influence of vegetation was diminished. This left the soil state to more directly control surface fluxes of moisture and energy. As a result, soil moisture was found to be a very influential surface variable for EF. Prior to harvest, the influence of LAI saturated at high values and the soil-air temperature gradient was found to be a valuable predictor of EF for winter wheat (Table 3). As shown in Figure 7f, increasing the soil-air temperature gradient corresponded to increasing sensible heat flux and lowering the EF. Combined with estimates of relative variable importance from the random forest analysis, this indicates that preharvest EF may be more strongly correlated with changes in sensible heat flux due to soil-air temperature differences than changes in evapotranspiration due to vegetation or soil moisture. However, our analysis cannot rule out that the air-soil temperature difference is a result of changing EF and not the cause. Regardless, this

provides evidence that the growth cycle and harvest timing of winter wheat have important implications for surface energy partitioning and potentially land-atmosphere coupling in this region, where ~30% of the land cover is winter wheat. While the influence of soil moisture or the temperature gradient increased or decreased depending on the state of winter wheat, the influence of explanatory variables on evaporative fraction at the grassland/pasture site was consistent across the growing season. LAI had the greatest influence followed distantly by soil moisture and soil-air temperature gradient. This does raise the question of why the relative influences of θ_v and T_{diff} on EF change between preharvest and postharvest periods. Prior to harvest, changes in winter wheat EF are strongly influence by T_{diff} (in addition to LAI). This is likely due to vegetation shading the soil and accessing deeper water for transpiration. As a result, the direct influence of the soil state on EF is reduced and changes in EF are more strongly influenced by changes in atmospheric conditions altering stomatal conductance and canopy evapotranspiration. After harvest, the vegetation buffer has been removed and soil is exposed to the atmosphere and its state more directly influences EF, leading to increased importance of soil moisture.

The differences in leaf area, evaporative fraction, and controls on evaporative fraction have important implications for studies of land-atmosphere coupling in the Southern Great Plains as winter wheat and grassland/pasture are the primary land cover types in the region. Further, these land cover types are not completely interspersed with each other. Instead, the western and eastern of portions of the SGP domain are primarily grassland/pasture, while the central portion of the domain is dominated by winter wheat cropland. Given the dependence of evaporative fraction on LAI and the dependence of LAI on land cover type and crop harvest timing, surface forcing could change with location within the SGP. Unfortunately, the combination of continuous observations of LAI and soil moisture observations does not exist at most other grassland/pasture and winter wheat sites in the SGP, so expanding this analysis from the central facility to all additional sites within the ARM SGP site is not currently feasible. However, we have shown that the changes in winter wheat EF between preharvest (mean EF ~ 0.55) and postharvest (mean EF ~ 0.34) across the region are analogous to the changes at the CF. This provides confidence that the results shown above for the CF are likely to extend across the region and are unlikely to be dependent on the years of data that were available for analysis.

Similar to *Williams and Torn* [2015], we found that increasing LAI tended to produce greater EF at the winter wheat site but that this effect saturated around 2.5 m^2 m^{-2} (Figure 7a). Additionally, consistent with *Ford et al.* [2014], we found that the relationship between θ_v and EF at the grassland/pasture site was only strong below ~0.28 m^3 m^{-3} LAI (e.g., Figure 8b). However, *Ford*

et al. [2014] also found that the relationship between soil moisture and EF was dependent on net radiation, with the EF-soil moisture relationship weakening at low radiation levels. Net radiation was not found to be an important variable in our analysis. Finally, the dependence of winter wheat and grassland/pasture EF on multiple environmental factors is similar to that found for wheat in Morocco by *Gentine et al.* [2007]. They found that EF is nearly independent of radiation and wind speed but dependent on soil moisture availability, canopy cover, and air-soil temperature gradients.

This analysis was limited to the Southern Great Plains of the United States. However, this study is relevant to other regions of the world, such as Europe and Central Asia, where winter crops with early summer harvest such as winter wheat, barley, and canola are grown [*Monfreda et al.*, 2008]. Also, potential future expansion of perennial crops such as those used for bioenergy production is likely to have phenology and rooting profiles that are unique relative to neighboring traditional crops and native vegetation [*Bagley et al.*, 2014b, 2015]. This could lead to agricultural scenarios similar to the landscapes investigated here, where different variables control evaporative fraction and influence land-atmosphere coupling on fields that are in close proximity to each other. Similarly, the potential addition of cover crops is likely to influence the postharvest surface energy balance. We hypothesize based that the addition of cover crops is likely to reduce the impact of winter wheat harvest on evaporative fraction relative to grassland/pasture, but further study is needed. Overall, the results presented here pose a challenge for models trying to accurately capture the dynamics of the land surface in regions that have heterogeneous landscapes with winter crop at subgrid scales. In particular, this study highlights the need to accurately model the planting, growth, and harvest cycles of agricultural crops, which are commonly simplified to generic C_3 or C_4 crop types in regional and global climate models and do not typically include winter crops [*Levis et al.*, 2012].

One limitation of this study is that the data available did not include any years with extremely low springtime soil moisture. During drought, soil moisture could become depleted throughout the rooting zone, and even in the presence of vegetation, soil moisture could control EF. It would be useful to test how these relationships are affected by extreme drought or pluvial years. Also the influence of other how climate and weather factors influence these results remains an open question. In particular, meteorological conditions that are amenable to particular strong or weak land-atmosphere coupling may lead to changes in the relative importance of surface variables on EF and may be worth future investigation. Finally, representative and reliable soil moisture measurements remain challenging. Recently, improved systems for measuring soil moisture and surface energy balance in the SGP have been implemented, and additional observations of

vegetation are ongoing. These emerging data sets may be suitable for additional tests of the robustness of our results, which would allow for more direct analysis of how the terrestrial component of land-atmosphere coupling is influenced by agriculture across the region.

5 Conclusion

With the prevalence of winter wheat and grassland/pasture in the Southern Great Plains, capturing winter wheat's growth cycle and harvest timing is crucial for properly representing the surface fluxes of the region, as well as other regions that have a similar mix of winter crops. Models that neglect the growth cycle of winter wheat and other winter crops are unlikely to correctly partition surface energy fluxes, which will have direct effects on atmospheric circulation and land-atmosphere coupling. Additionally, the surface variables that exert the most influence on EF differ between winter wheat and grassland/pasture and change when winter wheat has senesced and been harvested. Currently, few regional or global climate models include realistic representations of agricultural processes, and far fewer have developed validated routines for simulating winter crops such as winter wheat. These effects of land cover and agriculture should be included in regional and global models for accurate representation of surface energy partitioning and the water cycle in regions with a mix of winter crops such as the Southern Great Plains.

Acknowledgments

Data for the SGP sites were obtained from arm.gov from the following streams: sgp30co2flx4mmetC1.b1, sgp30baebbr, sgpswatsE.b1, sgpmfrsE13.b1, sgpmfrsC1.b1, and sgp30qcecor.b1. This research was supported by the Office of Biological and Environmental Research of the U.S. Department of Energy under contract DE-AC02-05CH11231 as part of the Atmospheric Radiation Measurement (ARM) and Atmospheric System Research (ASR) programs. Data supporting this research can be found at http://www.archive.arm.gov/.